

Numerical Investigation of the Influence of Shock Control Bumps on the Buffet Characteristics of a Transonic Airfoil

Steffen Bogdanski, Klemens Nübler, Thorsten Lutz and Ewald Krämer

Abstract This article presents a numerical investigation on the influence of three-dimensional shock control bumps (SCB) on the effect of transonic buffet. Three different types of SCBs are generated by an optimization for low drag in steady flow conditions at a medium lift coefficient. The impact of these SCB types is then investigated for two different Mach numbers with steady and unsteady RANS methods. It will be shown that all SCBs worsen buffet in terms of buffet onset and buffet amplitudes and shift the shock upstream. The impact is largely independent of the Mach number. Vortex strength and amount of separation in steady conditions are only poor indicators for the buffet inhibition potential of the bumps.

1 Introduction

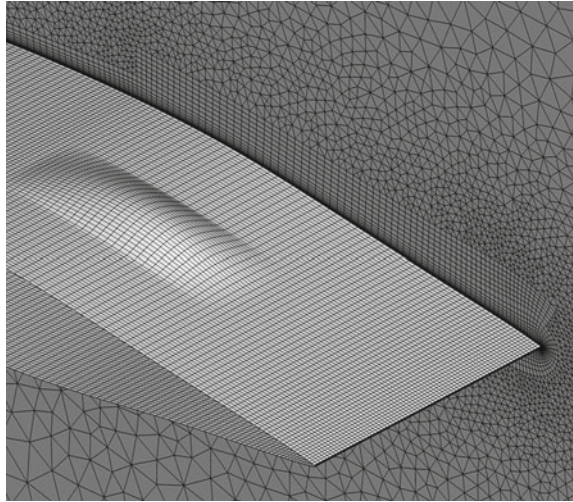
Two and three-dimensional shock control bumps (SCBs) have been investigated and optimized for numerous years at IAG. These SCBs expand the compression shock to a lambda-shock and reduce wave drag [1]. The main focus of the recent work has been on a robust bump design, i.e. a performance gain over a large range of lift coefficients, without performance deterioration in the design point of the baseline airfoil.

There are only few attempts to use SCBs to reduce the shock motion in transonic buffet [2]. All these attempts used steady computations for the design and evaluation of these “buffet bumps” and the criterion for the determination of the buffet onset has been the extend and shape of the separated flow rather than the unsteady behaviour [3].

It is the aim of this investigation to utilize steady and unsteady RANS methods to evaluate the impact of SCBs which are optimized for drag reduction on the buffet characteristics of a transonic airfoil. The investigation is conducted for two different Mach numbers: the design Mach number of the bumps and a smaller Mach number

S. Bogdanski (✉) · K. Nübler · T. Lutz · E. Krämer
Institute of Aerodynamics and Gas Dynamics, University of Stuttgart, 70569 Stuttgart, Germany
e-mail: bogdanski@iag.uni-stuttgart.de; <http://www.iag.uni-stuttgart.de>

Fig. 1 Surface grid and periodic boundary, coarse mesh



where the bumps are effective at a higher angle of attack, closer to the buffet onset. It can be supposed that bump design conditions closer to the buffet onset boundary will have a positive effect on the buffet characteristics.

2 Numerical Methods

The simulations presented in this chapter have been conducted with the unstructured CFD code “TAU” developed by the German Aerospace center (DLR) [4]. The code solves the Euler-, Navier-Stokes- or RANS-equations on grids with unstructured cells. It can be used for steady computations with various acceleration techniques as well as for unsteady computations with a second order dual time-stepping scheme. Several one-equation, two-equation and Reynolds stress turbulence models are implemented. All simulations in this chapter have been carried out with the “Menter SST” model with the “scale-adaptive simulation” modification (SST-SAS) [5].

The time step δt was chosen to $\frac{1}{40} \frac{c}{u_{inf}}$, with c as the chord length and u_{inf} as the free stream velocity. This leads to approximately 500 time steps per buffet period and has been proven to guarantee a time step independent solution [6]. Every fifth time step, a solution is preserved and used for post processing.

An implicit backward euler scheme has been used for the inner iterations with multi grid and residual smoothing. The flux discretization was realized with the second order Jameson, Schmidt, Turkel scheme.

For post processing purposes a python tool was written which extracts slices of the unsteady surface solution. The data of each slice and time step is then processed separately and values like lift, drag, shock position and extent of the separated area are

Table 1 Properties of the three grid levels (*Panel A*) and SCB positions x/c (*Panel B*)

Panel A: three grid levels			
	Fine	Medium	Coarse
Grid points	$4 \cdot 10^6$	$2 \cdot 10^6$	$1 \cdot 10^6$
Spanwise	121	96	76
Circumference	452	360	284
No. hexahedral layers	50	40	31
Extra prisms	10	8	6
Panel B: SCB positions			
	HSCB	Wedge	Extended
Begin	0.47	0.50	0.47
Crest	0.63	0.63	0.60
End	0.77	0.80	1.00

determined. These values are then integrated and time averaged. All post processing has been done with 25 slices equally spaced in spanwise direction and the tool has been verified against the results of the TAU solver.

2.1 Grids

Hybrid grids with structured hexahedral blocks for the boundary layer treatment and unstructured tetrahedral blocks for the treatment of the inviscid regions have been created with the commercially available software “Gridgen”. An additional structured block was created over the rear part of the airfoil to account for the thickened/separated boundary layer behind the shock. All grids have a spanwise extent of $0.3c$ and use periodic boundary conditions since these impose the least amount of artificial constraints on the flow solution Fig. 1.

Three different grid levels have been created to investigate the grid dependency of the solutions. The cell size was scaled with $\sqrt[3]{2}$ so as the overall amount of points doubles with each level. Table 1 (Panel A) shows the properties of each grid level and Fig. 1 shows the surface grid and one periodic boundary of the coarsest grid. The computations with the baseline airfoil have been carried out with both 2D and 3D grids, yet only minor differences occur in the solutions.

3 Results

3.1 Baseline Airfoil

The baseline airfoil originates from the Pathfinder transonic laminar wing [7] and has a thickness of 12.2%. The airfoil has been investigated for the two Mach numbers

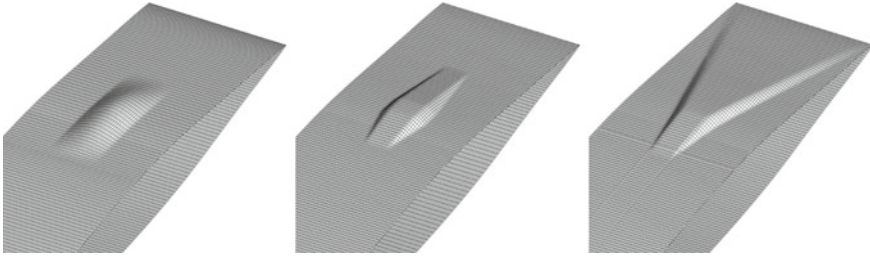


Fig. 2 Shape of the three bumps: HSCB, wedge and extended

$Ma = 0.74$ and $Ma = 0.76$ at a constant Reynolds number of $Re = 20 \cdot 10^6$. The transition was fixed at 10% of the chord length by limiting the production of turbulence in the laminar region. This leads to a boundary layer thickness near the shock comparable to that of wind tunnel test conducted in Cambridge. Steady solutions exist for all angles of attack with $\alpha \leq 4^\circ$ for $Ma = 0.76$ and $\alpha \leq 3^\circ$ for $Ma = 0.74$. Above these values transonic buffet occurs, with higher Mach number showing the smaller amplitudes.

With increasing angle of attack and shock strength the baseline airfoil develops a separation bubble at the location of the shock which is growing in streamwise direction. Once it reaches the trailing edge buffet occurs. This behaviour corresponds to “model A” according to the buffet classification of Pearcey [8].

3.2 Grid Dependency

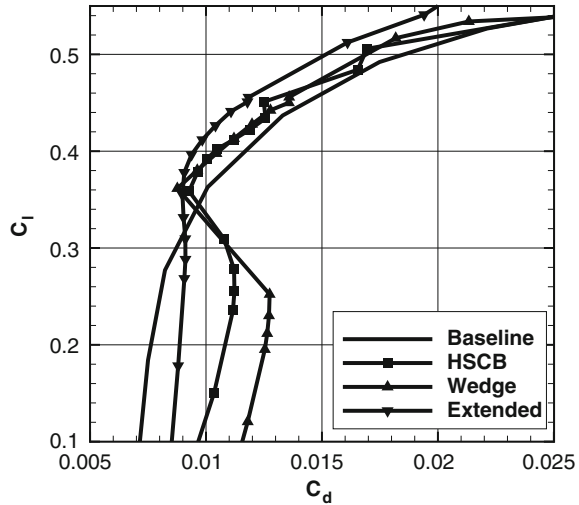
The grid dependency has been investigated for all geometries at the higher Mach number of $Ma = 0.76$. Though the differences between the different levels are small for conditions with attached flow, large differences occurred in the buffet regime. In general the finer grids reduced the buffet amplitudes but shifted the buffet onset to smaller angles of attack. The largest differences for the lift amplitudes of about a factor of 4 occurred between the coarse and medium grid, it is therefore mandatory that fine grids are used for reliable results.

3.3 Bump Generation

Three different bumps have been created for the Pathfinder airfoil: a smooth—hill shaped—one (HSCB), a wedge shaped one and an extended bump (see Fig. 2). A lift coefficient of $c_l = 0.417$ and a Mach number of $Ma = 0.76$ has been chosen as design point for all bumps.

The bumps have been optimized with a downhill simplex algorithm for minimal drag by variation of the two parameters height and position. The length of the smooth

Fig. 3 Drag polar for the three bumps, $Ma = 0.76$



and the wedge bump have been fixed at $l = 0.3 c$, whereas the extended bump varies in length and reaches the trailing edge for all designs. The spanwise extent of the wedge, the smooth and the front ramp of the extended bump have been fixed at $0.1 c$. When the performance of the three bumps is compared (see Fig. 3) it is evident, that the extended bumps shows the best performance at the design point. At off design conditions at lower lift coefficients the extended bump is superior to the two other bumps, too.

3.4 Impact of SCBs on Buffet at $Ma = 0.76$

Buffet Onset and Shock Motion All SCBs lower the buffet onset by an angle of attack of about 0.5° (see Fig. 4 left) and show larger buffet amplitudes inside the buffet regime than the baseline airfoil. However, it is not possible to determine the bump with the best/worst buffet behaviour since the buffet amplitudes vary with angle of attack.

The smooth and the extended bump shift the shock upstream, whereas the wedge bump shifts the shock downstream with regard to the baseline airfoil. During the buffet cycle the (spanwise averaged) shock positions stay above the front flank of the bumps, i.e. the bumps should influence the shock even in the buffet regime (compare Fig. 4 right with Table 1 Panel B).

Separation The HSCB and the wedge bump exhibit separated flow below the design point in contrast to the extended bump as shown in Fig. 5. This seems to be the reason for the better performance of the extended bump at lower lift coefficients. At design conditions almost no separation is apparent for all bumps. The amount of

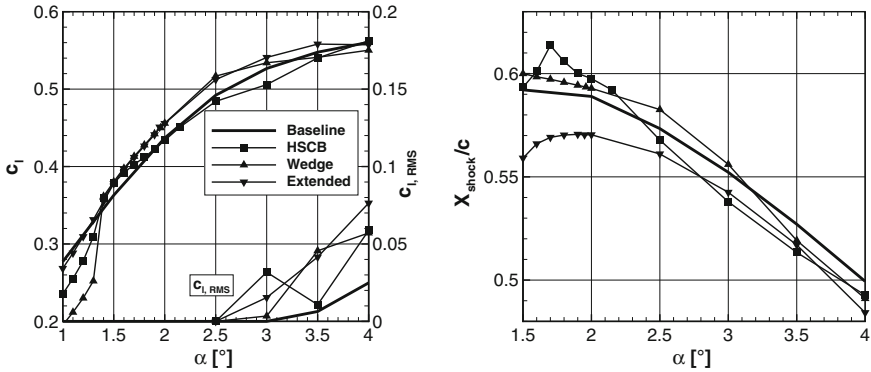
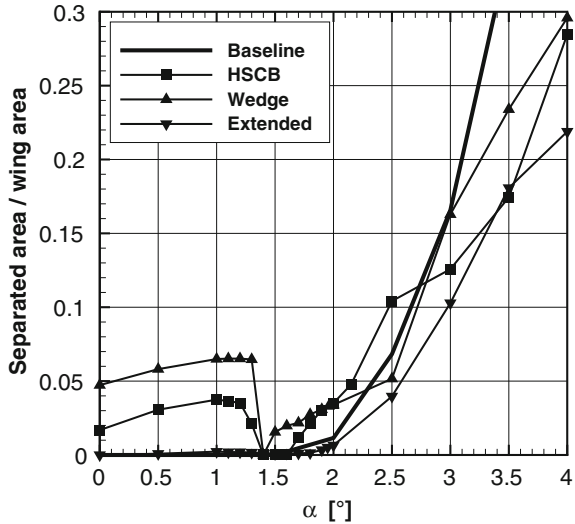


Fig. 4 Lift polar (left) and spanwise and temporally averaged shock position (right) for the three SCBs, $Ma = 0.76$

Fig. 5 Separated area over angle of attack for the three SCBs, $Ma = 0.76$



separation grows with increasing angle of attack for all bumps but it's not directly correlated with the amount of lift variation. Hence, the amount of separated flow at or above design conditions is not a good indication for determining buffet inhibition capabilities.

Vortex generation Figure 6 shows the vortex generation and the surface streamlines for the three bumps at design conditions. The slices show the x-component of the rotation $curl(v)$. At the end of the rear flank the wedge bump shows the largest values and thus creates the strongest vortices of all bumps. This is due to the separation at the rear flank and causes the vortices of the wedge bump to rotate in the opposite direction than the vortices on the other bumps. The HSCB and the extended bump

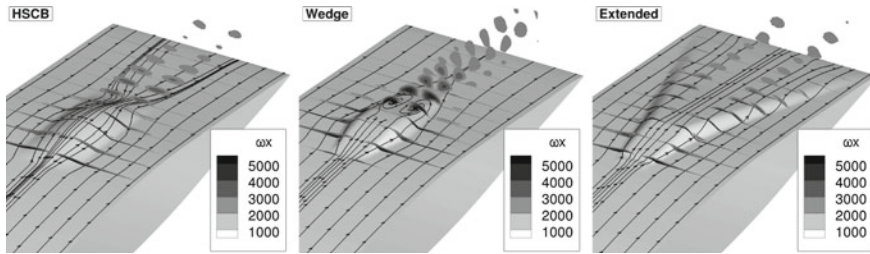


Fig. 6 Vortex generation for the three SCBs, $Ma = 0.76$, $\alpha = 1.5^\circ$

have similar peak values at this position, though the vortices of the extended bump are considerably flatter than those of the HSCB.

Since the SCBs show a similar buffet behaviour in terms of buffet onset and amplitudes it can be concluded, that the peak vorticity of the streamwise vortices is not correlated with the ability of the bump to inhibit buffet.

3.5 Impact of SCBs on Buffet at $Ma = 0.74$

When the freestream Mach number is lowered the shock moves upstream and likewise SCBs optimized for performance have to move in the same direction. The aforementioned bumps, optimized for the higher Mach number, are thus located too far downstream for good performance at medium lift coefficients. Their operating area is shifted towards higher lift coefficients, where the shock moves downstream to its original location. RANS computations showed that the new operation area is at a lift coefficient of $c_l \approx 0.6$. It can be presumed that bumps, which are effective in the vicinity of the buffet boundary, are more likely to enhance the buffet boundary. Since the wedge bump exhibited the worst off-design performance only the smooth and the extended bump are investigated at the lower Mach number.

Buffet onset and shock motion Figure 7 (left) shows that the smooth as well as the extended bump both deteriorate the buffet behaviour for the lower Mach number. The angle of attack for buffet onset is lowered about $\alpha = 0.5^\circ$ and the lift variations are considerably higher than those of the baseline airfoil. At least the maximum lift coefficient of the HSCB is slightly higher than that of the baseline airfoil, yet this point is already inside the buffet regime.

Figure 7 (right) shows the spanwise averaged shock positions. It can be seen that the shock is more upstream with regard to the bumps than for the higher Mach number. Thus a greater part of the bumps is located in the area with separated flow behind the shock and obviously less effective.

Separation At the lower Mach number separation starts before buffet onset (Fig. 8). The two bumps show a very similar development with the HSCB exhibiting approx.

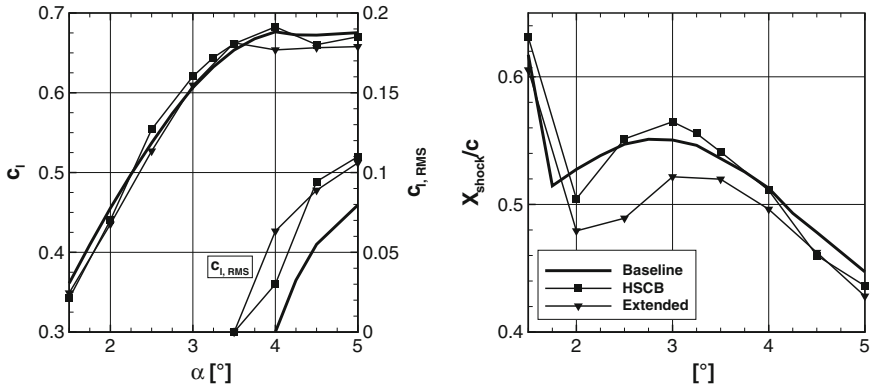
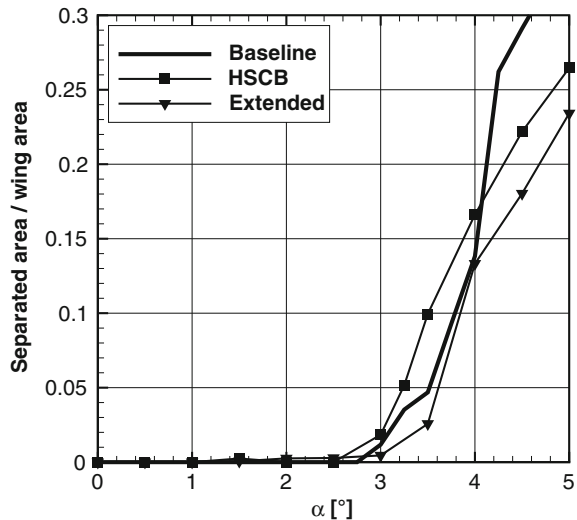


Fig. 7 Lift polar (left) and spanwise and temporally averaged shock position (right) at $Ma = 0.74$

Fig. 8 Separated area over angle of attack at $Ma = 0.74$



5% larger values, which is almost constant for higher angles of attack. Yet, inside the buffet regime the HSCB shows more separation than the baseline airfoil and the extended bump shows less than the baseline airfoil but both exhibit a similar buffet behaviour. For lower angles of attack almost no separation is visible for all configurations.

Vortex generation The vortices pictured in Fig. 9 are created at an angle of attack of $\alpha = 3.5^\circ$, which yields the last steady solution for both bumps. The HSCB generates a pair of considerably larger vortices than the Extended bump, though both exhibit almost the same buffet characteristics. When the surface streamlines of the HSCB are regarded first signs of asymmetry can be seen.

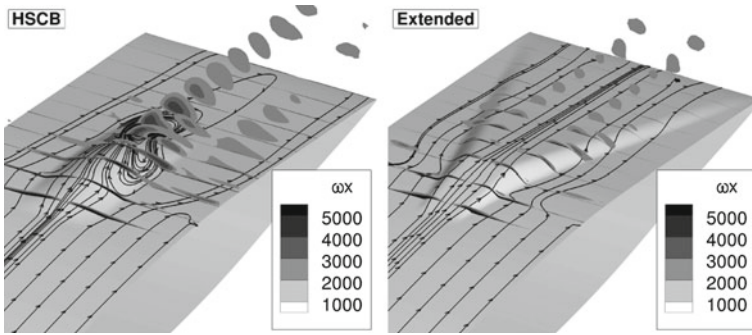


Fig. 9 Vortex generation for the three SCBs, $Ma = 0.74$, $\alpha = 3.5^\circ$

4 Conclusions

The buffet characteristics of three bumps have been investigated with URANS methods in the transonic flow regime. It has been shown, that fine grids are mandatory to keep the grid influence small. At the design Mach number all bumps deteriorate the buffet behaviour: they lower the angle of attack for buffet onset and lead to higher buffet amplitudes inside the buffet regime. The amount of separated flow and the vortex strength at steady conditions give only limited evidence of the buffet inhibition potential of a bump. The assumption, that a lower Mach number will be beneficial for the buffet characteristics of the bumps has been proven wrong. This behaviour is due to the fact that the bumps shift the shock upstream and thus lie in the area of separated flow behind the oscillating shock.

Notes and Comments.

The research leading to these results has received funding from the European Union’s Seventh Framework Programme (FP7/2007-2013) for the Clean Sky Joint Technology Initiative under grant agreement no. 271843.

References

1. Pätzold, M.: Auslegungsstudien zu 3D Shock-Control-Bumps mittels numerischer Optimierung. University of Stuttgart, Dissertation (2008)
2. Corre, C., et al.: Transonic flow control using a NS-solver and a multi-objective genetic algorithm. *Mech. Appl.* **73**, 297–302 (2003)
3. Eastwood, J., Jarett, J.: Towards designing with 3-D bumps for Wing Drag reduction. *AIAA* 2011–1168 (2011)
4. Gerhold, T.: Overview of the Hybrid RANS Code TAU. In: Kroll, N., Fassbender, J.K. (eds.) *Notes on Numerical Fluid Mechanics and Multidisciplinary Design*, Vol. 89, pp. 81–92. Springer, Heidelberg (2005)
5. Menter, F., Egorov, Y.: A scale-adaptive simulation model using two-equation models. *AIAA* 2005–1095 (2005)

6. Soda, A.: Numerical Investigation of Unsteady transonic Shock/boundary-Layer Interaction for Aeronautical Applications. Dissertation, RWTH Aachen (2006)
7. Streit, T., Horstmann, K.-H., Schrauf, G., Hein, S., Fey, U., Egami, Y., Perraud, J., El Din, I., Cella, U., Quest, J.: Complementary numerical and experimental data analysis of the ETW Telfona Pathfinder wing transition tests. 49th AIAA Aerospace Sciences Meeting, Orlando, AIAA Paper 2011-881 (2011)
8. Pearcey, H., Osborne, J.: The Interaction between Local Effects at the Shock and Rear Separation a Source of Significant Scale Effects in Wind-Tunnel Tests on Airfoils and Wings. AGARD, CP35 (1968)